Evidence of early microstructural white matter abnormalities in multiple sclerosis from multi-shell diffusion MRI

Silvia De Santis[a,b], Tobias Granberg[c,d,e], Russell Ouellette[c,e], Constantina A. Treaba[e], Elena Herranz[e], Qiuyun Fan[e], Caterina Mainero[e,1], Nicola Toschi[e,f,*,1]

[a] Instituto de Neurociencias de Alicante (CSIC-UMH), San Juan de Alicante, Spain
[b] Cardiff University Brain Research Imaging Centre (CUBRIC), Cardiff University, Cardiff, UK
[c] Department of Clinical Neuroscience, Karolinska Institutet, Stockholm, Sweden
[d] Department of Radiology, Karolinska University Hospital, Stockholm, Sweden
[e] Athinoula A. Martinos Center for Biomedical Imaging and Harvard Medical School, Boston, MA, USA.
[f] Department of Biomedicine and Prevention, University of Rome Tor Vergata, Rome, Italy

ARTICLE INFO

ABSTRACT

Irreversible white matter (WM) damage, including severe demyelination and axonal loss, is a main determinant of long-term disability in multiple sclerosis (MS). Non-invasive detection of changes in microstructural WM integrity in the disease is challenging since commonly used imaging metrics lack the necessary sensitivity, especially in the early phase of the disease. This study aims at assessing microstructural WM abnormalities in early-stage MS by using ultra-high gradient strength multi-shell diffusion MRI and the restricted signal fraction (FR) from the Composite Hindered and Restricted Model of Diffusion (CHARMED), a metric sensitive to the volume fraction of axons.

In 22 early MS subjects (disease duration ≤ 5 years) and 15 age-matched healthy controls, restricted fraction estimates were obtained through the CHARMED model along with conventional Diffusion Tensor Imaging (DTI) metrics. All imaging parameters were compared cross-sectionally between the MS subjects and controls both in WM lesions and normal-appearing white matter (NAWM).

We found a significant reduction in FR focally in WM lesions and widespread in the NAWM in MS patients relative to controls (corrected $p < .05$). Signal fraction changes in NAWM were not driven by perilesional tissue, nor were they influenced by proximity to the ventricles, challenging the hypothesis of an outside-in pathological process driven by CSF-mediated immune cytotoxic factors. No significant differences were found in conventional DTI parameters. In a cross-validated classification task, FR showed the largest effect size and outperformed all other diffusion imaging metrics in discerning lesions from contralateral NAWM.

Taken together, our data provide evidence for the presence of widespread microstructural changes in the NAWM in early MS stages that are, at least in part, unrelated to focal demyelinating lesions. Interestingly, these pathological changes were not yet detectable by conventional diffusion imaging at this early disease stage, highlighting the sensitivity and value of multi-shell diffusion imaging for better characterizing axonal microstructure in MS.

1. Introduction

Multiple sclerosis (MS) is a chronic inflammatory demyelinating and neurodegenerative disease of the central nervous system. While axonal degeneration is the major predictor of long-term disability (Lee et al., 2014), its underlying mechanisms are still unclear. Inflammatory demyelination has been traditionally considered the underlying cause of axonal loss, however, recent evidence indicates that it may also be induced by other causes (Brück, 2005), including direct cytotoxic attack, antibody-mediated mechanisms, dysfunctional glial-neuronal crosstalk and exposure to glutamate and cytokines (Haines et al., 2011).

Non-invasive in vivo characterization of microstructural WM integrity in MS is challenging, particularly in early disease stages. Traditional neuroimaging approaches based on volumetry of grey and

white matter (WM) from MRI scans are sensitive only to macroscopic atrophy, and should be employed with caution when evaluating short-term disease progression in individual patients (Miller et al., 2002), also given that atrophy mostly develops over longer timescales as opposed to microstructural tissue changes. More advanced imaging measures, including proton magnetic resonance spectroscopy of *N*-acetylaspartate, are more specific to axonal damage (De Stefano et al., 1998; Sajja et al., 2009), but have limited spatial resolution.

Using Diffusion Tensor Imaging (DTI, Basser et al., 1994), an MRI technique that measures properties of the diffusion process which are associated to microstructural properties of brain tissue, abnormalities in diffusivity have been detected in focal MS lesions, normal-appearing WM (NAWM), and grey matter (Werring et al., 1999). Such alterations correlate with physical disability (Filippi et al., 2001) and with cognitive impairment (Rovaris et al., 2002) in cohorts with heterogeneous disease duration. Diffusion tensor imaging derived indices, however, are relatively unspecific and sensitive to a number of microstructural tissue characteristics including myelination, axonal density and, amongst others, to the presence of crossing fibers (Beaulieu, 2002; De Santis et al., 2014a,b). In MS, demyelination, axonal loss and fiber orientation dispersion have similar impact on DTI indices, and can therefore not be differentiated (Wheeler-Kingshott and Cercignani, 2009).

Advanced multi-shell diffusion-weighted imaging methods, including the Neurite Orientation Dispersion and Density Imaging (NODDI; Zhang et al., 2012) and the Composite Hindered and Restricted Model of Diffusion (CHARMED; Assaf and Basser, 2005) models, address these limitations by separating different intra- and extracellular compartments and thereby producing the restricted signal fraction (FR), an imaging parameter sensitive to the volume fraction of axons. It has been recently pointed out, however, that some of these multi-compartment diffusion models, including NODDI, may be biased, especially in pathological tissue, by the tortuosity assumption that affects the estimation of the restricted diffusion compartment (Lampinen et al., 2016). In this study, by using the CHARMED model we do not rely on the tortuosity approximation and therefore estimate indices that are considered a reliable surrogate marker of microstructural WM abnormalities (Assaf and Basser, 2005).

While a handful of previous studies have looked into the benefits of multi-shell MRI in MS (Assaf et al., 2002; Kipp et al., 2016; Cross and Song, 2017), these investigations were limited by the maximum achievable angular resolution and/or gradient strength, and included individuals with heterogeneous disease duration, resulting in a lack of specific information about microstructural WM damage in early disease stages. A pioneering pilot study in a small ($n = 6$) MS cohort demonstrated the benefits of multi-shell diffusion-weighted imaging in assessing axonal integrity (Huang et al., 2016) by focusing on the corpus callosum only. A few multi-shell diffusion imaging studies used the NODDI model to investigate grey matter (Granberg et al., 2017), spinal cord (By et al., 2017) and WM (Granberg et al., 2017; Schneider et al., 2017). However, recent work has shown that the interpretation of NODDI results in terms of axonal pathology might be biased in WM due to specific model assumptions (Lampinen et al., 2016).

Here, we employed whole-brain multi-shell diffusion-weighted MRI at high angular resolution and gradient strength to characterize WM lesions and NAWM in early MS. We hypothesized that CHARMED would disclose an early reduction in FR in WM lesions and NAWM, and that this model would be more sensitive than conventional DTI metrics in detecting WM pathology in early disease stages. We also aimed at assessing NAWM FR alterations while excluding perilesional tissue to investigate whether the observed microstructural changes are mostly driven by proximity to focal demyelinating lesions or involve more widespread processes. Finally, we studied NAWM FR as a function of distance from the ventricles to assess whether FR reduction could be associated with CSF-mediated inflammatory factors, which have been implied in driving WM tissue changes as measured by magnetization transfer ratio (Brown et al., 2017).

2. Materials and methods

2.1. Subjects

The local institutional review board approved this study and written informed consent was obtained from all participants. We prospectively enrolled 22 MS subjects and 15 age-matched healthy controls. General inclusion criteria were: age 18–60 years, absence of significant medical history (other than MS for patients) and of MRI contraindications. Eligibility criteria in patients included a diagnosis of relapsing-remitting MS (Polman et al., 2011; Lublin et al., 2014) with a disease duration ≤ 5 years in line with previous work (Chard and Miller, 2009), being on stable disease-modifying treatment or no treatment for at least 3 months, absence of clinical relapse within 3 months and absence of corticosteroids use within one month from study enrollment. Physical disability was assessed by a neurologist according to the Expanded Disability Status Scale (EDSS; Kurtzke, 1983). In addition, four healthy controls (one female, three males; mean age 35.3 years, standard deviation 8.8 years) were recruited for assessing the scan-rescan reproducibility of all diffusion metrics. Demographic and clinical data are shown in Table 1.

2.2. Data acquisition

All subjects underwent a multi-shell diffusion MRI protocol on an ultra-high gradient 3 T scanner (Siemens Healthcare, Erlangen, Germany), featuring a novel gradient system equipped with 300 mT/m maximum gradient strength (Fan et al., 2016) and a custom-made 64-channel head coil (Keil et al., 2013). Diffusion-weighted imaging was acquired using a spin-echo echo-planar sequence with the following parameters: repetition/echo time 8800/57 ms, δ/Δ 12.9/21.8 ms, field of view 210 × 210 mm, isotropic voxel size 1.5 mm^3, 96 slices. Three diffusion weightings (b-values) were applied along non-collinear gradient directions: 1000 (64 directions), 5000 (128 directions) and 10,000 s/mm^2 (128 directions). In addition, 28 diffusion un-weighted scans (b0 images) were acquired, interspersed throughout the diffusion-weighted scans to facilitate motion correction. This protocol is suited for both conventional DTI and CHARMED analysis (De Santis, 2013). Additional imaging sequences acquired for lesion segmentations were a 3D T$_1$-weighted Multi-Echo Magnetization-Prepared Rapid Gradient Echo (van der Kouwe et al., 2008) with the following parameters: flip angle 7°, repetition time 2530 ms, echo times 1.15–3.03-4.89-6.75 ms,

Table 1
Demographic and clinical characteristics of the analyzed cohort.

	MS	Controls
Mean age (SD), years	39.4 (8.6)	38.3 (11.3)
Sex	18 females, 4 males	8 females, 7 males
Disease duration in years (1st-3rd quartile)	2.5 (1.6–3.3)	–
Median EDSS score (minimum-maximum)	2.0 (0.0–4.0)	–
Treatment	dimethyl fumarate (10), glatiramer acetate (4), interferon beta-1a (4), natalizumab (1), no treatment (3)	–

Abbreviations: EDSS = expanded disability status scale; MS = multiple sclerosis, HC = healthy controls.

inversion time 1100 ms; and a 3D T$_2$-weighted Fluid-Attenuated Inversion Recovery (FLAIR) with the following parameters: variable flip angle, repetition time 5000 ms, echo time 393 ms, inversion time 1800 ms. Both the T$_1$-weighted and FLAIR scans had isotropic voxel size 1 mm^3, 176 slices, and a generalized auto-calibrating partially parallel acquisitions (GRAPPA) acceleration factor 2.

2.3. Data processing

The T$_1$-weighted images were pre-processed for gradient non-linearity correction and processed through the Freesurfer cortical reconstruction stream. (v. 5.3.0, http://freesurfer.net, Fischl, 2012). Topological surface reconstruction defects caused by WM and/or leukocortical lesions were corrected with semi-automatic lesion in-painting in FreeSurfer. Lesion in-painting and quality control was performed by an expert radiologist starting from the Freesurfer segmentations. This entailed visual inspection and manual in-painting as well as corrections of lesions that were missed or erroneously classified by the automated segmentation procedure. Diffusion-weighted data were pre-processed with tools in FreeSurfer and FSL (v. 5.0, http://fsl.fmrib.ox.ac.uk/fsl/fslwiki/). Diffusion pre-processing included gradient non-linearity correction, motion correction and eddy current correction including b-matrix reorientation. Additional details are available at: http://www.humanconnectome.org/documentation/MGH-diffusion/.

The lower b-value shell (b = 1000 s/mm^2) along with b0 images was used to run DTI analysis using ExploreDTI (v.4.8.4, http://www.exploredti.com/; Leemans et al., 2009). In this analysis, the tensor model was fitted using a Robust Estimation of Tensors by Outlier Rejection approach (Chang et al., 2005), after which the following maps were computed for each subject: fractional anisotropy (FA), mean diffusivity (MD), axial diffusivity (AD) and radial diffusivity (RD). All diffusion shells were employed to fit the CHARMED model (Assaf and Basser, 2005) using in-house software written in MATLAB R2015b (The MathWorks, Natick, MA, USA). The CHARMED model separates the contribution of the signal originating from the extra-axonal space that undergoes hindered diffusion, and the signal originating from the intra-axonal space that undergoes restricted diffusion, as shown in Fig. 1. The total signal fraction of the restricted compartment (FR) is sensitive to axonal volume fraction. The fitting routine employs non-linear least square to fit the data to the CHARMED model and estimate the total restricted signal fraction of the axonal compartments, the orientation of the axonal compartments, the diffusivity of the axonal compartment and the extra-axonal tensor; the initial values fed to the fitting routine are: FR = 0.3, orientation [0 pi/2], diffusivity = $1*10^{-3}$ m^2/s for each fiber, and diffusion tensor [0.3 0.3 1.2 0 0 0]. After fitting the CHARMED model FR maps were extracted for all subjects.

The CHARMED model separates the contribution of the signal originating from the extra-axonal space, which undergoes hindered diffusion (in red), and the signal originating from the intra-axonal space, which undergoes restricted diffusion (in blue) by explicitly modeling
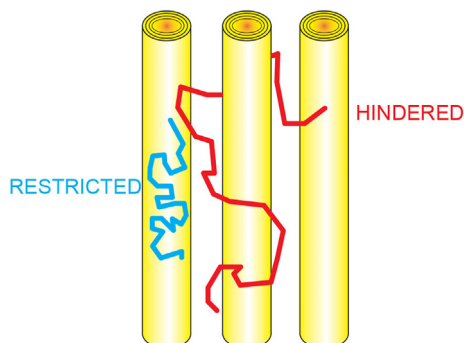

Fig. 1. Hindered and restricted signal in the CHARMED model.

the two compartments with different analytical probability distribution functions (Assaf and Basser, 2015).

Abbreviations: CHARMED = Composite Hindered and Restricted ModEl of Diffusion

2.4. Lesion, white matter and ventricular masks

The topological surface reconstructions created in Freesurfer were used for creating anatomical masks of the cortex, WM and CSF. The following global segmentation metrics were also extracted: total intracranial volume, total grey matter volume, total white matter volume. In MS subjects, lesions were segmented on tFLAIR images using a semi-automated method in 3D Slicer (v. 4.2.0, https://www.slicer.org/) by an expert radiologist (CAT).

In order to compare the lesions with a topographically homologous region, the corresponding non-lesioned contralateral region was segmented by applying a non-linear transform of the 3D T$_1$-weighted image and its corresponding right-left flipped mirror image to the MNI152 template. This was followed by visual inspection of the images to exclude possible lesional tissue from the contralateral mask. Additionally, perilesional masks were created by expanding original lesion masks perpendicular to the lesion surface by one and two voxels respectively in three dimensions using a Gaussian kernel and median dilation (see Fig. 3A). These masks were employed to investigate the contribution of the perilesional tissue to the group differences observed in NAWM (see below). Finally, periventricular WM masks were also obtained based on FreeSurfer segmentations of the lateral ventricles from which six layers of concentrically expanding, 1-voxel thick, masks surrounding the ventricles were created (see Fig. 3A), also obtained by expanding the masks in three dimensions using a Gaussian kernel and median dilation. The resulting masks were multiplied by the WM mask, in order to only consider WM voxels in the analysis and avoid partial volume effects. These concentric periventricular masks were employed to investigate a putative influence of the soluble inflammatory factors present in the CSF on group differences in CHARMED indices. In order to minimize direct CSF contamination, the layer immediately adjacent to the ventricles was excluded. The non-diffusion-weighted echo-planar images were registered to the FreeSurfer reconstructions using boundary-based registration with 12 degrees-of-freedom, and this served as a transformation for the aforementioned anatomical masks into diffusion space.

2.5. Data analysis

2.5.1. Voxel-wise comparison between MS and controls in NAWM

Fractional anisotropy maps computed through the DTI models were fed into an in-house modified version of the Tract-Based Spatial Statistics (TBSS) routine of FSL (Smith et al., 2006), in which the normalization to MNI standard space is performed using more accurate registration tools (ANTs package, http://stnava.github.io/ANTs/; Klein et al., 2009). The registration employs lesion masks to exclude lesions from the optimization procedure that calculates warp fields. After skeleton extraction, skeletonized maps were obtained for all parameters and general linear model (GLM) was used within a voxel-wise, permutation-based, non-parametric statistical framework (Smith et al., 2006) to test for differences in NAWM between MS and controls, while excluding voxel-wise lesion masks on an individual patient bases and controlling for age, gender and multiple comparisons across clusters using Threshold Free Cluster Enhancement (TFCE). We employed 10,000 permutations, and a corrected voxel-wise p-value < .05 was considered statistically significant. Automatic localization of significant clusters was performed using the Jülich Histological Atlas (Eickhoff et al., 2005) and reviewed by a radiology expert (TG). In order to test correlation between imaging parameters and the EDSS, the same analysis was repeated for the MS cohort only, by including EDSS as an independent predictor in the GLM. Given that DTI and CHARMED
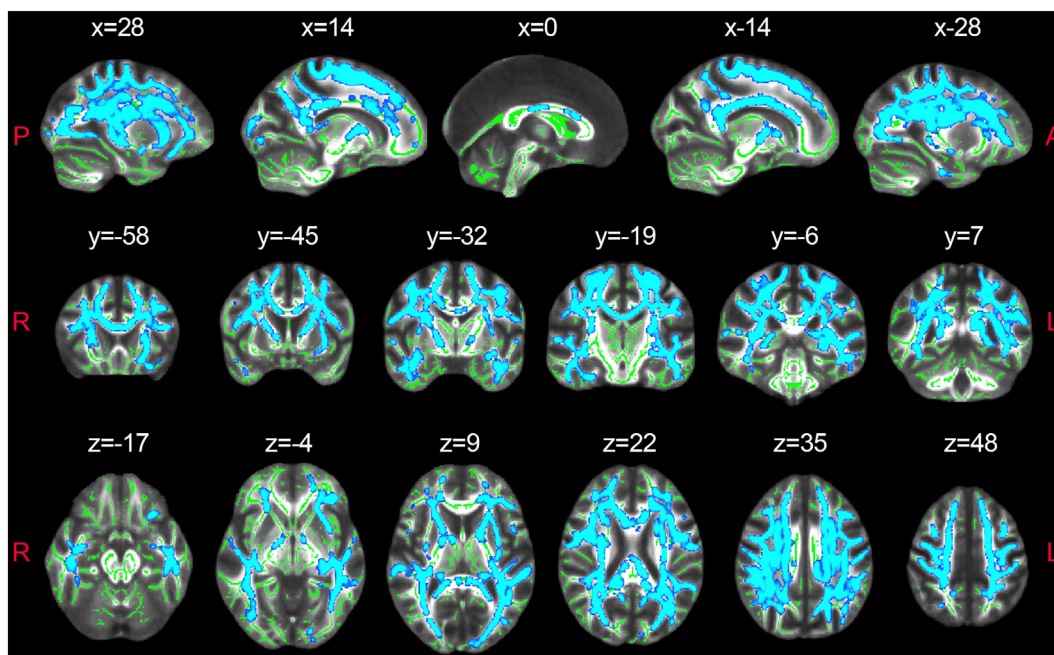
Fig. 2. CHARMED-FR reductions in multiple sclerosis normal appearing white matter.
Regions (highlighted in blue) in which TBSS found significantly lower FR in multiple sclerosis NAWM compared to healthy controls.
Abbreviations: FR = restricted fraction; NAWM = normal-appearing white matter. The skeleton generated by TBSS analysis is highlighted in green

models employ different numbers of gradient orientations, we repeated the CHARMED analysis using a subset of the total number of gradient orientations, optimally chosen to maximize the b-value and shell coverage (De Santis et al., 2014a,b).

2.5.2. Contribution of perilesional tissue to group-wise differences

Whenever we observed significant differences in NAWM between the MS and control groups, we repeated statistical analysis twice after expanding the lesion masks by one as well as two voxels to investigate the contribution of perilesional tissue to the observed differences in NAWM.

2.5.3. Influence of proximity to the ventricles on the difference in imaging parameters

For all the indices we calculated the mean value within the five concentric 1-voxel thick periventricular masks described above. Repeated measures ANalysis Of Variance (r-ANOVA) was then used to assess the effect of the distance from the ventricles on the observed differences between NAWM in MS patients and controls (within-subject factor: distance from ventricles, between-subject factor: group. The model also included a group*distance interaction term).

2.5.4. Comparison between MS lesions and contralateral NAWM

For each MS patient of the cross-sectional cohort, the mean value for each parameter K = {FA, MD, RD, AD, FR} was calculated in native space both within each lesion and within the corresponding contralateral NAWM (CLNAWM) region. Given that different anatomical locations present different baseline values for each parameter, we defined a summary statistic (normalized index of asymmetry, NIA) as follows in order to render differences between lesions and contralateral NAWM comparable across regions:

$$NIA(LESION\ vs.CLNAWM) = \frac{(K_{LESION} - K_{CLNAWM})}{(K_{LESION} + K_{CLNAWM})} \quad (1)$$

where K_{LESION} is the average of parameter K within each lesion and K_{CLNAWM} is the average of parameter K within the corresponding contralateral NAWM region of interest. NIA ranges from 1 (maximum asymmetry towards the lesion) through 0 (no asymmetry) to −1

(maximum asymmetry towards the contralateral NAWM). The null hypothesis of no asymmetry (i.e. NIA = 0) was then tested across patients through a nonparametric signed-rank test, followed by Bonferroni correction for multiple comparisons across indices.

2.5.5. Discriminatory ability of each parameter in discerning lesions

In order to establish the predictive power of each parameter in detecting microstructural alterations (i.e. lesions) within MS patients, a set of logistic classifiers were trained in a 10-fold cross-validation setting to discern lesions from contralateral NAWM values using the software package Weka v3.8 (Trapp et al., 1999). Receiver operating characteristic (ROC) curves were then generated by varying the threshold on the class probability estimates. Finally, as aggregate measures of performance, we employed sensitivity, specificity, positive predictive value and the area under the ROC curve (AUC).

2.5.6. Scan-rescan reproducibility of diffusion metrics

Since CHARMED has not yet been employed for clinical applications, the scan-rescan reproducibility of all diffusion metrics, both in the cortex and in white matter, was assessed in four healthy volunteers by acquiring the diffusion-weighted scans twice, in the same day, with a short time interval between the two imaging sessions, and with re-positioning of subjects between scans. Data was processed as described earlier and the FA maps for each subject's second scan was linearly registered (12 degrees-of-freedom) to the FA maps from the first scan. For each subject, the coefficient of variations (CoV) was estimated voxel-wise as the ratio between the standard deviation and the mean of each pair (Scan 1, Scan 2) of measurements. A separate TBSS routine was applied in this cohort to extract the WM skeleton and the CoV was projected onto the skeleton. Within-subject CoV in the skeleton was calculated by averaging the values in the skeleton mask.

2.5.7. Global segmentation measures

Group-wise comparisons (HC vs. MS) in global segmentation measures normalized by total intracranial volume were performed using non-parametric Mann-Whitney-U tests.

3. Results

3.1. Voxel-wise comparison between MS and healthy controls in NAWM and correlations with physical disability

We found lower FR in the NAWM of the MS group relative to controls (Fig. 2). The differences were symmetrical across hemispheres and involved all major WM tracts, notably: the anterior thalamic radiation, the corticospinal tract, the cingulum of the cingulate cortex and hippocampus and the inferior fronto-occipital, uncinate, inferior and superior longitudinal fasciculi. Interestingly, no DTI parameters showed significant differences in this analysis. Furthermore, we found negative voxel-wise correlations between EDSS and both FA and FR, which however did not survive multiple comparison correction across the skeleton (data not shown). In Supplementary Figure 1, we show that even when the CHARMED analysis is repeated using only 64 gradient orientations, there are significant differences in FR between healthy controls and MS patients in a number of WM areas.

3.2. Contribution of perilesional tissue to the observed difference in microstructure between MS and controls in NAWM

When excluding perilesional tissue from the voxel-wise statistical analysis of group differences, findings remained largely unchanged (Fig. 3), indicating that the observed lower estimated FR in NAWM of MS subjects relative to controls was not only present in, or driven exclusively by, perilesional areas.

Left: Example of the lesion mask expansion by one and two voxels (panel A). Right: Results (highlighted in blue) in which TBSS found a significant reduction of the FR in multiple sclerosis NAWM compared to healthy controls for the original lesion masks (panel B), for the masks expanded by one voxel (panel C, volumetric overlap of regions with significant differences as compared to analysis b: 98%), and for the masks expanded by two voxels (panel D, volumetric overlap of regions with significant differences as compared to analysis b: 96%), are shown.

Abbreviations: FR = restricted fraction; NAWM = normal-appearing white matter; TBSS = Tract based Spatial Statistics

3.3. Group differences in estimated FR as a function of distance from CSF

Repeated measures ANalysis Of Variance demonstrated a significant effect of both distance ($p < .001$, decreasing values of FR as distance increases from the ventricles) and group ($p = .001$, lower FR in MS subjects relative to controls, in accordance with TBSS results). The interaction effect (group*distance) was, however, not statistically significant (Fig. 4), suggesting that there is no direct effect of proximity to the ventricles on the difference in FR between MS patients and controls. None of the other indices displayed a significant group*distance effect (data not shown).

Example of the ventricle mask as well as surrounding concentric periventricular masks (overlaid on fractional anisotropy map) at perpendicular distances from the ventricles ranging from 1 to 6 voxels (panel a). Panel b shows box-whisker plots of restricted fraction values in each layer (distance from ventricles: from 2 to 6 voxels; the first layer was excluded in order to minimize cerebrospinal fluid contamination). Boxes represent quartiles, whiskers represent extremes, crosses represent outliers. Repeated measures analysis of variance found an effect of both group ($p < .001$) and distance ($p < .001$), but not of group*distance interaction ($p = .78$).

3.4. Comparison between MS lesions and contralateral NAWM

Statistically significant asymmetries between lesions and contralateral NAWM were detected in all indices (Fig. 5). FR consistently showed the greatest asymmetry, reflecting the greatest contrast in lesioned tissue, across all indices tested.

3.5. Discriminatory ability in discerning lesions

The precision, sensitivity and specificity of the imaging metrics in discriminating lesions from NAWM are summarized in Table 2. DTI indices performed satisfactorily (area under the ROC curve 0.75–0.85), however FR yielded the single highest area under the ROC curve (0.90) and precision (0.79) as well as the highest specificity (0.80). Fig. 6 shows the ROC curves for all parameters and analyses.

3.6. Scan-rescan reproducibility of diffusion metrics

The average CoV for all diffusion metrics is shown in Fig. 7 and was smaller than 10.2% for all diffusion metrics.
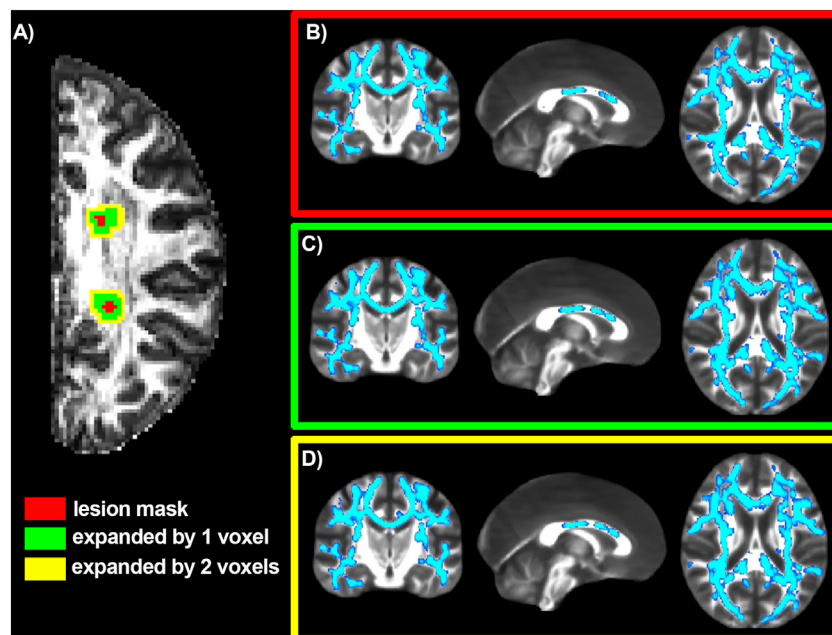
Fig. 3. CHARMED-FR reductions in multiple sclerosis normal appearing white matter excluding perilesional tissue.

Example of the lesion mask expansion by one and two voxels (panel A). Right: Results (highlighted in blue) in which TBSS found a significant reduction of the FR in multiple sclerosis NAWM compared to healthy controls for the original lesion masks (panel B), for the masks expanded by one voxel (panel C, volumetric overlap of regions with significant differences as compared to analysis b: 98%), and for the masks expanded by two voxels (panel D, volumetric overlap of regions with significant differences as compared to analysis b: 96%), are shown.

Abbreviations: FR = restricted fraction; NAWM = normal-appearing white matter; TBSS = Tract Based Spatial Statistics.
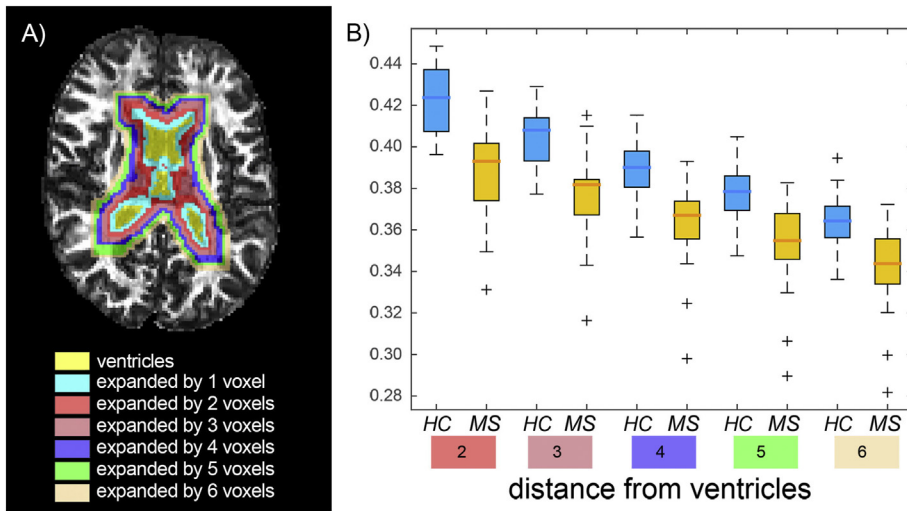
Fig. 4. Restricted fraction in periventricular area. Example of the ventricle mask as well as surrounding concentric periventricular masks (overlaid on fractional anisotropy map) at perpendicular distances from the ventricles ranging from 1 to 6 voxels (panel a). Panel b shows box[HYPHEN]whisker plots of restricted fraction values in each layer (distance from ventricles: from 2 to 6 voxels; the first layer was excluded in order to minimize cerebrospinal fluid contamination). Boxes represent quartiles, whiskers represent extremes, crosses represent outliers. Repeated measures analysis of variance found an effect of both group ($p < 0.001$) and distance ($p < 0.001$), but not of group*distance interaction ($p = 0.78$).
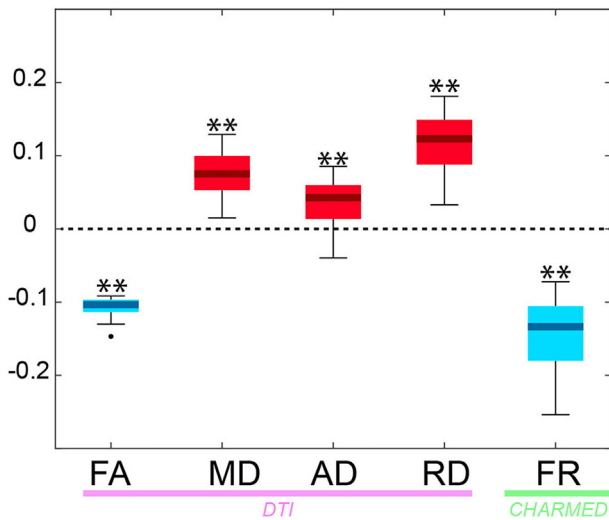

Fig. 5. Asymmetry index in MS vs NAWM.
Box-whisker plots depicting the asymmetry index NIA between MS lesions and contralateral NAWM (1: maximum asymmetry towards the lesion, -1: maximum asymmetry towards contralateral NAWM or healthy controls) across patients. Red: positive NIA (** = $p < .01$, Bonferroni corrected). Blue: negative NIA (** = $p < .01$, Bonferroni corrected). Boxes represent quartiles, whiskers represent extremes, dots represent outliers.
Abbreviations: FR = restricted fraction; NAWM = normal-appearing white matter; NIA = normalized index of asymmetry

Fig. 6. Receiver operating characteristic curves.
ROC curves for the performance of parameters FA, MD, AD, RD and FR in discriminating lesions from contralateral NAWM. Dashed black line indicates no predictive power above chance discrimination.
Abbreviations: ROC = receiver operating characteristic; AD = axial diffusivity; FA = fractional anisotropy; FR = restricted fraction; MD = mean diffusivity; NAWM = normal-appearing white matter; RD = radial diffusivity

Table 2
AUROC, sensitivity, specificity and positive predictive value obtained when discerning lesions from contralateral NAWM and from controls using a logistic classifier trained within a 10-fold cross-validation procedure.

	Performance (LESION/CLNAWM)				
	FA	MD	AD	RD	FR
AUROC	0.75	0.85	0.70	0.85	0.90
Sensitivity	0.79/0.70	0.79/0.75	0.70/0.67	0.79/0.75	0.79/0.79
Specificity	0.71/0.80	0.75/0.79	0.67/0.71	0.75/0.79	0.80/0.80
Positive Predictive value	0.73/0.77	0.76/0.78	0.68/0.69	0.76/0.78	0.79/0.79

Abbreviations: AUROC = Area under Receiver Operating Characteristic curve; NAWM = Normal-Appearing White Matter; FA = Fractional Anisotropy; MD = Mean Diffusivity; AD = Axial Diffusivity; RD = Radial Diffusivity; FR = Restricted Fraction.
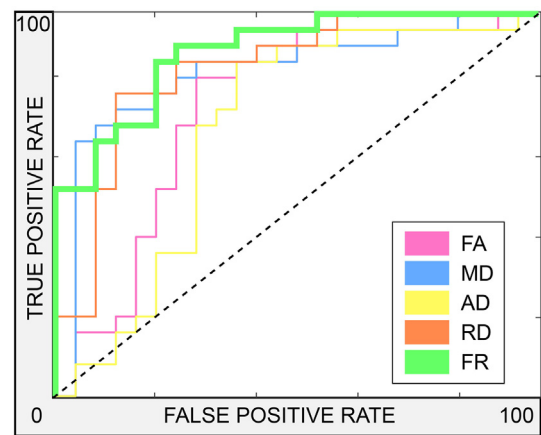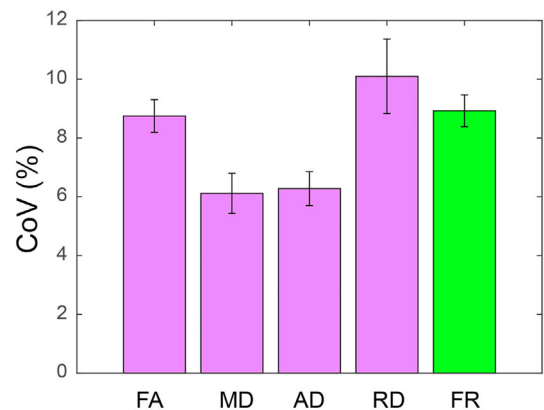

Fig. 7. Average coefficient of variation for diffusion metrics.
The averaged CoV, calculated on the WM skeleton, and the corresponding standard deviation are shown as percentage for the diffusion metrics FA, MD, AD, RD and FR.
Abbreviations: CoV = coefficient of variation; FA = fractional anisotropy; MD = mean diffusivity; AD = axial diffusivity; RD = radial diffusivity; FR = restricted fraction; WM = white matter

3.7. Global segmentation measures

p-values related to these comparisons were as follows: total grey matter volume (normalized by total intracranial volume): $p = .73$, total white matter volume (normalized by total intracranial volume): $p = .70$. We can therefore exclude that global scaling effects may have driven our local results.

4. Discussion

In this study, the combined use of an MRI scanner equipped with a ultra-high strength gradient system with compartment-specific modeling approaches allowed us to perform a targeted, non-invasive, whole-brain in vivo investigation of microstructural tissue alterations in MS. We demonstrated a widespread reduction of the restricted signal fraction FR in WM lesions and in NAWM in early stage MS that could not be detected with conventional DTI. While axonal loss is an important component of MS pathology and a main determinant of long-term disability and disease progression (Lee et al., 2014), diffusion-based approaches with better sensitivity to axonal microstructure as compared to DTI have only recently started to emerge (Kipp et al., 2016; Cross and Song, 2017; Huang et al., 2016). Early, non-invasive detection of axonal changes in MS is valuable for identifying patients at high risk of disease progression and, potentially, for understanding disease mechanisms of axonal damage and assess the effects of neuro-protective treatments. Pathological data suggest that inflammatory axonal transection in acute lesions and lack of myelin-trophic support in chronically demyelinated lesions may be responsible for axonal loss in early disease stages (Trapp et al., 1999; Kuhlmann et al., 2002; Frank et al., 2014). In advanced stages, primary neurodegenerative mechanisms and energy failure have also been hypothesized to underlie progressive accumulation of diffuse axonal damage (Criste et al., 2014).

By excluding perilesional tissue in the analysis of FR changes in the NAWM of MS subjects, we demonstrated that the widespread reduction of FR was not strictly driven by changes located in close proximity to focal WM lesions. This finding indicates that, in early MS stages, WM changes in NAWM expand beyond local inflammatory lesions visible on conventional MRI. Recent animal work (Singh et al., 2017), showed that interfering with Wallerian degeneration in inflammatory demyelination does not suffice to prevent acute axonal damage and, eventually, irreversible axonal loss. Interestingly, while axonal loss could also be due to Wallerian degeneration happening distal to lesions, these experimental data showed that the highest numbers of axons undergoing Wallerian degeneration is located in perilesional WM early in the disease course (Singh et al., 2017), hence mitigating this possible confound in the interpretations of our results.

In this study, we also investigated changes in FR, in the MS cohort relative to controls, as a function of distance from the ventricles. Previous data disclosed the presence of a gradient in magnetization transfer ratio abnormalities, suggestive of underlying demyelination, from periventricular to deep NAWM in a heterogeneous MS population, with the most marked abnormality seen in the immediate periventricular region (Brown et al., 2017). The same pattern was observed in early MS stages and interpreted as being consistent with a CSF- or ependymal-mediated pathogenesis for NAWM demyelination (Liu et al., 2015). Also, a gradient in the expression of cortical pathology as evidenced by increase in quantitative T_2^* at 7 T, indicative of myelin and iron loss, has been previously demonstrated throughout MS stages (Mainero et al., 2015). Here, we found that FR decreased, in both the MS and the control group, as a function of distance from the ventricles, possibly reflecting generally increased axonal density and myelination in the central WM relative to subcortical regions. Interestingly, although the FR was lower in MS compared to controls at all distances, this difference was statistically independent from the distance from the ventricles. While the previously cited studies employed different/simpler statistical approaches (i.e. either univariate statistics at each

distance point or a linear fit prior to statistical comparison) to assess the impact of the distance from the ventricles, our findings weaken the hypothesis that an outside-in pathological process, possibly mediated by CSF soluble inflammatory mediators, plays an exclusive role in driving the observed changes. Taken together, our data are compatible with the presence of distinct patterns for demyelination and axonal degeneration in the NAWM of MS, and, as shown by pathological and experimental work (Brück, 2005) imply a multifactorial pathogenesis for WM changes not necessarily directly linked to inflammatory demyelination, even in early disease stages. Additional pathogenetic factors may include retrograde axonal degeneration from degenerating cortical neurons, or early mitochondrial dysfunction (Su et al., 2009).

The use of diffusion MRI to separate the effects of demyelination, axonal loss and fiber dispersion in WM has been previously suggested (Budde et al., 2009), and DTI-derived radial and axial diffusivity have been proposed as putative markers for demyelination and axonal loss respectively. However, DTI is inherently insufficient to disentangle these pathways of disease progression. Radial and axial diffusivity are mutually dependent and are influenced by the underlying fiber architecture and specifically by the amount of crossing fibers present in the voxel (Wheeler-Kingshott and Cercignani, 2009; De Santis et al., 2014a,b).

We also showed the increased sensitivity of CHARMED-derived estimates, relative to DTI, in detecting significant differences between MS and controls in NAWM and between lesions and NAWM in MS patients. In NAWM, DTI indices failed to detect significant microstructural differences in this early MS cohort. The lack of significant differences in NAWM between patients and controls in DTI indices is in agreement with existing cross-sectional literature, which suggests DTI lacks sensitivity in detecting subtle changes at the early disease stages (Griffin et al., 2001) and that much larger sample sizes are needed to detect a significant effect (Deppe et al., 2016). Importantly, in this study, we showed that the lack of sensitivity of DTI is not due to the fact that it employs a shorter data acquisition protocol, but is instead inherent to the model itself. In keeping with this hypothesis, we observed significant group-wise FR differences in areas known to include a large fraction of crossing fibers, such as the centrum semiovale and the uncinate fasciculus, where DTI is known to provide limited sensitivity. In contrast, the CHARMED model explicitly models multiple possible distinct orientations and can therefor correctly highlight differences in such areas.

In agreement with current DTI literature, we found significant DTI differences in lesions compared to contralateral and healthy tissue. However, in this analysis FR was associated with the largest effect size. In addition, FR returned the best performance in discriminating lesions from NAWM in a cross-validated classification task. Taken together, these evidences suggest that CHARMED outperforms conventional DTI as a marker to detect microstructural changes also in lesions, and therefore holds promise as a novel tool for early diagnosis and disease-monitoring purposes.

In our work, EDSS was only significantly correlated with FR at an uncorrected level. While this finding could be due to the low level of disability (and hence also low variability) of this early MS cohort, the current study demonstrates the potential significance of advanced imaging tools in the early detection of irreversible tissue damage.

This study has several potential limitations. The CHARMED model was originally designed to mainly capture variation in the size of the restricted water pool, with the intent of providing a surrogate marker for axonal density. However, since the restricted fraction is normalized with respect to the total water content (both extra and intracellular) it is possible that also changes in myelination, or variations in the total water content, could affect the CHARMED restricted fraction. As such, since we are not separately assessing demyelination, the conclusions on axonal pathology being independent of demyelination are partly speculative, and micro-inflammatory processes in NAWM (e.g. involving microglia) cannot be excluded. It is also important to point out that,

while the CHARMED model is often quoted to provide volume fractions, it also relies on the assumption that the proton density and the relaxation rates are the same in all compartments. Given that this assumption has been disputed both in normal tissue (Veraart et al., 2017), and in disease (Lampinen et al., 2018), in this paper we refer to FR as a signal fraction.

Additionally, our findings about FR as a function of distance could be slightly biased by intrinsically different ROI sizes as distance varies. Also, the CHARMED model, while accounting for crossing fibers, does not explicitly account for an orientation dispersion factor around the principal directions. Specifically, fiber dispersion appears to be important in areas characterized by mainly one orientation (Ronen et al., 2014; Mollink et al., 2017) while the commonly employed Watson distribution around a single principal orientation appears unsuitable to capture true fiber arrangement in areas of fiber crossing (Mollink et al., 2017). It is likely that both fiber crossing and dispersion should be included in a more sophisticated model in order to better describe the variability in diffusion signal observed in-vivo.

The CHARMED model appears to provide enhanced sensitivity as compared to traditional DTI. However, the biological states and pathological processes that contribute to the FR estimates (e.g. axonal damage but also possibly edema or ischemia) remain to be further validated in animal models and/or in ex vivo investigations. With reference to our study, it is important to note that there is no evidence of ischemia in early MS. Additionally, edema could also be reflected, at least to a certain extent, by DTI MD changes (in concordance with our findings in lesions but not in NAWM).

The high-end setup used in this study is likely to play a role in the ability to characterize the subtle changes happening in this very early stage of the disease, which could be more difficult to see with the same level of significance in a clinical setup. However, a CHARMED protocol suitable for clinical needs is currently available (De Santis et al., 2014a,b). Recent results showed that it can discriminate between MS lesions, NAWM and healthy control tissue (De Santis et al., 2018), hence simultaneously providing enhanced sensitivity to both microstructural and macroscopically visible tissue alterations.

Funding

Appendix A. Supplementary data

Supplementary data to this article can be found online at https://doi.org/10.1016/j.nicl.2019.101699.

References

Assaf, Y., Basser, P.J., 2005. Composite hindered and restricted model of diffusion (CHARMED) MR imaging of the human brain. NeuroImage 27, 48–58.

Assaf, Y., Ben-Bashat, D., Chapman, J., Peled, S., Biton, I.E., Kafri, M., et al., 2002. High b-value q-space analyzed diffusion-weighted MRI: Application to multiple sclerosis. Magn. Res. Med. 47, 115–126.

Basser, P.J., Mattiello, J., LeBihan, D., 1994. Estimation of the effective self-diffusion tensor from the NMR spin echo. J. Magn. Reson. B 103, 247–254.

Beaulieu, C., 2002. The basis of anisotropic water diffusion in the nervous system - a technical review. NMR Biomed. 15, 435–455.

Brown, J.W., Pardini, M., Brownlee, W.J., Fernando, K., Samson, R.S., Prados Carrasco, F., et al., 2017. An abnormal periventricular magnetization transfer ratio gradient occurs early in multiple sclerosis. Brain 140, 387–398.

Brück, W., 2005. Inflammatory demyelination is not central to the pathogenesis of multiple sclerosis. J. Neurol. 252, V10–V15.

Budde, M.D., Xie, M., Cross, A.H., Song, S.K., 2009. Axial diffusivity is the primary correlate of axonal injury in the experimental autoimmune encephalomyelitis spinal cord: a quantitative pixelwise analysis. J. Neurosci. 29 (9), 2805–2813.

By, S., Xu, J., Box, B.A., Bagnato, F.R., Smith, S.A., 2017. Application and evaluation of NODDI in the cervical spinal cord of multiple sclerosis patients. Neuroimage Clin. 15, 333–334.

Chang, L.C., Jones, D.K., Pierpaoli, C., 2005. RESTORE: robust estimation of tensors by outlier rejection. Magn. Reson. Med. 53, 1088–1095.

Chard, D., Miller, D., 2009. Grey matter pathology in clinically early multiple sclerosis: evidence from magnetic resonance imaging. J. Neurol. Sci. 282, 5–11.

Criste, G., Trapp, B., Dutta, R., 2014. Axonal loss in multiple sclerosis: causes and mechanisms. Handb Clin. Neurol. 122, 101–113.

Cross, A.H., Song, S.K., 2017. A new imaging modality to non-invasively assess multiple sclerosis pathology. J. Neuroimmunol. 304, 81–85.

De Santis, S., 2013. Diffusion MR imaging: how to get the maximum from the experimental time. Transl. Neurosci. 4, 59–65.

De Santis, S., Assaf, Y., Evans, C.J., Jones, D.K., 2014a. Improved precision in CHARMED assessment of white matter through sampling scheme optimization and model parsimony testing. Magn. Res. Med. 71, 661–671.

De Santis, S., Drakesmith, M., Bells, S., Assaf, Y., Jones, D.K., 2014b. Why diffusion tensor MRI does well only some of the time: variance and covariance of white matter tissue microstructure attributes in the living human brain. NeuroImage 89, 35–44.

De Santis, S., Bastiani, M., Droby, A., Kolber, P., Pracht, E., Stoecker, T., Zipp, F., Groppa, S., Roebroeck, A., 2018. Characterizing white matter degeneration in multiple sclerosis: the impact of experimental design on advanced diffusion MRI biomarkers. Neuroscience. https://doi.org/10.1016/j.neuroscience.2018.03.048. (in press).

De Stefano, N., Matthews, P.M., Fu, L., Narayanan, S., Stanley, J., Francis, G.S., et al., 1998. Axonal damage correlates with disability in patients with relapsing-remitting multiple sclerosis. Results of a longitudinal magnetic resonance spectroscopy study. Brain 121, 1469–1477.

Deppe, M., Tabelow, K., Krämer, J., Tenberge, J.G., Schiffler, P., Bittner, S., et al., 2016. Evidence for early, non-lesional cerebellar damage in patients with multiple sclerosis: DTI measures correlate with disability, atrophy, and disease duration. Mult. Scler. 22 (1), 73–84.

Eickhoff, S.B., Stephan, K.E., Mohlberg, H., Grefkes, C., Fink, G.R., Amunts, K., et al., 2005. A new SPM toolbox for combining probabilistic cytoarchitectonic maps and functional imaging data. NeuroImage 25, 1325–1335.

Fan, Q., Witzel, T., Nummenmaa, A., Van Dijk, K.R., Van Horn, J.D., Drews, M.K., et al., 2016. MGH-USC human connectome project datasets with ultra-high b-value diffusion MRI. NeuroImage 124, 1108–1114.

Filippi, M., Cercignani, M., Inglese, M., Horsfield, M.A., Comi, G., 2001. Diffusion tensor magnetic resonance imaging in multiple sclerosis. Neurology 56, 304–311.

Fischl, B., 2012. FreeSurfer. NeuroImage 62, 774–781.

Frank, E., Hall, M., Trigg, L., Holmes, G., Witten, I., 2014. Data mining in bioinformatics using WEKA. Bioinformatics 20, 2479–2481.

Granberg, T., Fan, Q., Treaba, C.A., Ouellette, R., Herranz, E., Mangeat, G., et al., 2017. In vivo characterization of cortical and white matter neuroaxonal pathology in early multiple sclerosis. Brain 140, 2912–2926.

Griffin, C.M., Chard, D.T., Ciccarelli, O., Kapoor, R., Barker, G.J., Thompson, A.I., et al., 2001. Diffusion tensor imaging in early relapsing-remitting multiple sclerosis. Mult. Scler. 7 (5), 290–297.

Zhang, H., Schneider, T., Wheeler-Kingshott, C.A., Alexander, D.C., 2012. NODDI: practical in vivo neurite orientation dispersion and density imaging of the human brain. NeuroImage 16, 1000–1016.

Haines, J.D., Inglese, M., Casaccia, P., 2011. Axonal damage in multiple sclerosis. Mt Sinai J. Med. 78, 231–243.

Huang, S.Y., Tobyne, S.M., Nummenmaa, A., Witzel, T., Wald, L.L., McNab, J.A., 2016. Characterization of axonal disease in patients with multiple sclerosis using high-gradient-diffusion MR imaging. Radiology 280, 244–251.

Keil, B., Blau, J.N., Biber, S., Hoecht, P., Tountcheva, V., Setsompop, K., et al., 2013. A 64-channel 3T array coil for accelerated brain MRI. Magn. Reson. Med. 70, 248–258.

Kipp, L., Cawley, L., Prados, F., 2016. Neurite orientation dispersion and density imaging (NODDI) in RRMS. Neurology 86 (4), 159.

Klein, A., Andersson, J., Ardekani, B.A., Ashburner, J., Avants, B., Chiang, M.C., et al., 2009. Evaluation of 14 nonlinear deformation algorithms applied to human brain MRI registration. NeuroImage 46, 786–802.

Kuhlmann, T., Lingfeld, G., Bitsch, A., Schuchardt, J., Brück, W., 2002. Acute axonal damage in multiple sclerosis is most extensive in early disease stages and decreases over time. Brain 125, 2202–2212.

Kurtzke, J.F., 1983. Rating neurologic impairment in multiple sclerosis. An expanded disability status scale (EDSS). Neurology 33, 1444–1452.

Lampinen, B., Szczepankiewicz, F., Novén, M., van Westen, D., Hansson, O., Englund, E., Mårtensson, J., Westin, C.F., Nilsson, M., 2018. Can the neurite density be estimated with diffusion MRI? A multidimensional MRI study using b-tensor encoding and multiple echo times. pp. 18062731.

Lampinen, B., Szczepankiewicz, P., Mårtensson, J., van Westen, D., Sundgren, P.C., Nilsson, M., 2016. Neurite density imaging versus imaging of microscopic anisotropy in diffusion MRI: a model comparison using spherical tensor encoding. NeuroImage 147, 517–531.

Lee, J.Y., Taghian, K., Petratos, S., 2014. Axonal degeneration in multiple sclerosis: can

we predict and prevent permanent disability? Acta Neuropathol. Commun. 2, 97.

Leemans, A., Jeurissen, B., Sijbers, J., Jones, D.K., 2009. Explore DTI: a graphical toolbox for processing, analyzing, and visualizing diffusion MR data. In: Proceedings of the 17th Scientific meeting, International Society for Magnetic Resonance in Medicine, Honolulu, USA, pp. 3537.

Liu, Z., Pardini, M., Yaldizli, O., Sethi, V., Muhlert, N., Wheeler-Kingshott, C.A., et al., 2015. Magnetization transfer ratio measures in normal-appearing white matter show periventricular gradient abnormalities in multiple sclerosis. Brain 138, 1239–1246.

Lublin, F.D., Reingold, S.C., Cohen, J.A., Cutter, G.R., Sørensen, P.S., Thompson, A.J., et al., 2014. Defining the clinical course of multiple sclerosis. Neurology 83, 278–286.

Mainero, C., Louapre, C., Govindarajan, S.T., Giannì, C., Nielsen, A.S., Cohen-Adad, J., et al., 2015. A gradient in cortical pathology in multiple sclerosis by in vivo quantitative 7 T imaging. Brain 138, 932–945.

Miller, D.H., Barkhof, F., Frank, J.A., Parker, G.J.M., Thompson, A.J., 2002. Measurement of atrophy in multiple sclerosis: pathological basis, methodological aspects and clinical relevance. Brain 125, 1676–1695.

Mollink, J., Kleinnijenhuis, M., Cappellen van Walsum, A.V., Sotiropoulos, S.N., Cottaar, M., Mirfin, C., Heinrich, M.P., Jenkinson, M., Pallebage-Gamarallage, M., Ansorge, O., Jbabdi, S., Miller, K.L., 2017. Evaluating fibre orientation dispersion in white matter: comparison of diffusion MRI, histology and polarized light imaging. NeuroImage 15 (157), 561–574.

Polman, C.H., Reingold, S.C., Banwell, B., Clanet, M., Cohen, J.A., Filippi, M., et al., 2011. Diagnostic criteria for multiple sclerosis: 2010 Revisions to the McDonald criteria. Ann. Neurol. 69, 292–302.

Ronen, I., Budde, M., Ercan, E., Annese, J., Techawiboonwong, A., Webb, A., 2014. Microstructural organization of axons in the human corpus callosum quantified by diffusion-weighted magnetic resonance spectroscopy of N-acetylaspartate and post-mortem histology. Brain Struct. Funct. 219, 1773–1785.

Rovaris, M., Iannucci, G., Falautano, M., Possa, F., Martinelli, V., Comi, G., et al., 2002. Cognitive dysfunction in patients with mildly disabling relapsing-remitting multiple sclerosis: an exploratory study with diffusion tensor MR imaging. J. Neurol. Sci. 195, 103–109.

Sajja, B.R., Wolinsky, J.S., Narayana, P.A., 2009. Proton magnetic resonance spectroscopy in multiple sclerosis. Neuroimaging Clin. N. Am. 19, 45–58.

Schneider, T., Brownlee, W., Zhang, H., Ciccarelli, O., Miller, D.H., Wheeler-Kingshott, C.G., 2017. Sensitivity of multi-shell NODDI to multiple sclerosis white matter changes: a pilot study. Funct. Neurol. 32, 97–101.

Singh, S., Dallenga, T., Winkler, A., Roemer, S., Maruschak, B., Siebert, H., et al., 2017. Relationship of acute axonal damage, Wallerian degeneration, and clinical disability in multiple sclerosis. J. Neuroinflammation 14 (1), 57.

Smith, S.M., Jenkinson, M., Johansen-Berg, H., Rueckert, D., Nichols, T.E., Mackay, C.E., et al., 2006. Tract-based spatial statistics: voxelwise analysis of multi-subject diffusion data. NeuroImage 31, 1487–1505.

Su, K.G., Banker, G., Bourdette, D., Forte, M., 2009. Axonal degeneration in multiple sclerosis: the mitochondrial hypothesis. Curr. Neurol. Neurosci. Rep. 9 (5), 411–417.

Trapp, B.D., Ransohoff, R., Rudick, R., 1999. Axonal pathology in multiple sclerosis: relationship to neurologic disability. Curr. Opin. Neurol. 12 (3), 295–302.

van der Kouwe, A.J., Benner, T., Salat, D.H., Fischl, B., 2008. Brain morphometry with multiecho MPRAGE. NeuroImage 40, 559–569.

Veraart, J., Novikov, D.S., Fieremans, E., 2017. TE dependent diffusion imaging (TEdDI) distinguishes between compartmental T2 relaxation times. NeuroImage 182, 360–369 (pii: S1053-8119(17) 30778-4).

Werring, D.J., Clark, C.A., Barker, G.J., Thompson, A.J., Miller, D.H., 1999. Diffusion tensor imaging of lesions and normal-appearing white matter in multiple sclerosis. Neurology 52, 1626–1632.

Wheeler-Kingshott, C.A.M., Cercignani, M., 2009. About "axial" and "radial" diffusivities. Magn. Res. Med. 61, 1255–1260.